View metadata, citation and similar papers at core.ac.uk
brought to you by CORE
provided by Digital.CSIC

PHYSICAL REVIEW B **69**, 094306 (2004)

# Pressure dependence of the lattice dynamics of ZnO: An *ab initio* approach

J. Serrano,[1] A. H. Romero,[2] F. J. Manjón,[3] R. Lauck,[1] M. Cardona,[1,*] and A. Rubio[4]
[1]*Max Planck Institut für Festkörperforschung, Heisenbergstrasse 1, D-70569 Stuttgart, Germany*
[2]*Advanced Materials Department, IPICyT, Camino a la presa San José 2055, 78216 San Luis Potosí, San Luis Potosi, Mexico*
[3]*Departamento de Física Aplicada, Universitat Politècnica de València, EPSA, ES-03801 Alcoy, Spain*
[4]*Departamento Física de Materiales, Facultad de Ciencias Químicas, Universidad del País Vasco, Centro Mixto CSIC-UPV/EHU and Donostia International Physics Center, E-20018 San Sebastián, Basque Country, Spain*
(Received 20 November 2003; published 30 March 2004)

We have performed first-principles calculations of the electronic structure of ZnO, and applied them to the determination of structural and lattice-dynamical properties and their dependence on pressure. The dynamical matrices have been obtained for the wurtzite, zinc-blende, and rocksalt modifications with several lattice parameters optimized for pressures up to 12 GPa. These matrices are employed to calculate the one-phonon densities of states (DOS) and the two-phonon DOS associated with either sums or differences of phonons. These results provide the essential tools to analyze the effect of isotope-induced mass disorder and anharmonicity on phonon linewidths, which we discuss here and compare with experimental data from Raman spectroscopy, including first- and second-order spectra. Agreement of calculated properties with experimental results improves considerably when the renormalization due to anharmonicity is subtracted from the experimental data.

DOI: 10.1103/PhysRevB.69.094306 PACS number(s): 63.20.−e, 78.20.Bh, 78.30.Fs

## I. INTRODUCTION

Zinc oxide, the mineral zincite, crystallizes under normal conditions with the wurtzite structure (wz), which corresponds to the space group $P6_3mc$. Its applications in industry extend to many fields, such as pharmacy, where it is used as basic ingredient for preparation of cosmetics, uv-absorbing sun lotions, and diverse wound healing balsams. Other known applications[1,2] cover the production of adhesive tapes, tire rubber, varistors, ceramics, glass, and even animal feed.[3,4] Recently, it has attracted increasing interest because of its electronic properties, i.e., a semiconducting band gap of $\approx$3.4 eV, and the possibilities for application in optoelectronic devices, directly or as a substrate for the growth of other semiconductors such as GaN and SiC.[5] Therefore these properties have been extensively characterized, both from the experimental[5,6] and the theoretical[7–11] points of view. However, despite the existence of large natural zincite crystals, and also synthetic ones,[12] our knowledge of the vibrational properties of this material is rather limited. This fact poses an obstacle to our understanding of the transport properties, especially the thermal conductivity, which are of importance in the development of high quality optoelectronic devices.

As a wurtzite crystal, ZnO has phonon-dispersion relations consisting of 12 branches whose group-theoretical analysis at the Brillouin-zone center ($\mathbf{q}=0$) yields a decomposition into $2A_1+2B_1+2E_1+2E_2$, where $E_1$ and $E_2$ are double degenerate modes. The zero-frequency acoustic phonons correspond to one $E_1$ and one $A_1$ mode. ZnO is surprising in the sense that no complete experimental data set is available for the phonon-dispersion relations, despite the availability of large enough crystals. Inelastic neutron-scattering (INS) data for ZnO have been reported only for the acoustic branches.[13–15] Besides these data, there are several publications concerning the Raman spectra of ZnO (Refs. 16–19) as a function of temperature[20] and pressure,[21,22] which still cannot provide information about the $B_1$ mode (at $\mathbf{q}=0$), since it is infrared (ir) and Raman inactive. The theoretical description of the lattice dynamics through semiempirical models,[15] fitted to the few experimental data available, is somewhat questionable.

Another issue concerning the properties of this material is its phase diagram. The growth of ZnO in the zinc-blende structure (zb) could improve the possibilities for optoelectronic devices, as it may be the case for AlN and GaN.[23] However, ZnO grows as a bulk crystal in the wurtzite modification only, which undergoes a transition with pressure to the rocksalt (rs) phase at $\approx$8 GPa.[24–26] Epitaxial films with zinc-blende structure have been grown on GaAs substrates[27] and thin films of this structure have been reported by Bragg and Darbyshire.[28] Recently, growth of nanocrystalline rocksalt ZnO during a pressure cycle has been also reported.[29]

In this work we use first-principles calculations based on density-functional theory to investigate the lattice dynamics of ZnO for three phases: wurtzite, zinc blende, and rocksalt, under different hydrostatic pressures. The calculations have been performed using the method of linear response within density-functional perturbation theory.[30,31] We report calculations of the phonon dispersion relations for the three investigated phases, as well as a detailed analysis of the one- and two-phonon densities of states, which can successfully reproduce recent experimental observations by Raman measurements under pressure on samples with several isotopic compositions.[32] The calculated dispersion relations and densities of states (DOS) are also useful for the interpretation of extant second-order Raman data.

## II. COMPUTATIONAL METHOD

The *ab initio* calculations were performed with the code ABINIT, based on density-functional theory using the pseudopotential method and a plane-wave expansion of the wave functions.[33–35] The pseudopotentials were generated using the Troullier-Martins scheme,[36] treating the $3d$ electrons of

 ©2004 The American Physical Society

TABLE I. Calculated structural parameters of wurtzite-ZnO compared with both experimental and theoretical data reported in the literature. The table lists the calculated values for the equilibrium volume per unit formula at zero pressure $V_0$ (in Å$^3$) the lattice parameters $a$ and $c$ (in Å), the structural and internal parameters of the unit cell for the wurtzite phase $c/a$ and $u$, and $B_0$ (in GPa) and $B'$ which stand for the bulk modulus and its pressure derivative at $V_0$. The values in parentheses denote the error bars of the experimental data. For anharmonic corrections to these data see text in Sec. III. See Sec. III A for a discussion about the importance of the anharmonic renormalization of the structural parameters concerning the comparison between experimental and calculated data.

| | $V_0$ | $a$ | $c$ | $c/a$ | $u$ | $B_0$ | $B'$ |
|---|---|---|---|---|---|---|---|
| | | | | Wurzite | | | |
| This work | 22.882 | 3.198 | 5.167 | 1.615 | 0.379 | 159.5 | 4.5 |
| Expt. [a] | 23.796(11) | 3.2496(6) | 5.2042(20) | 1.6018(7) | 0.3819(1) [c] | 183(7) | 4 |
| Expt. [b] | 23.810(6) | 3.2498(3) | 5.2066(3) | 1.6021(3) | 0.3832(2) | 142.6(2) | 3.6 |
| Theor. [d] | 24.570 | 3.290 | 5.241 | 1.593 | 0.3856 | 154.4 | 3.6 |
| Theor. [e] | 22.874 | 3.199 | 5.163 | 1.6138 | 0.3790 | 162.3 | 4.05 |
| | | | | Rocksalt | | | |
| This work | 18.856 | 4.225 | | | | 209.1 | 2.7 |
| Expt. [a, f] | 19.484(11) | 4.271(2) | | | | 228(7) | 4 |
| Expt. [b, f] | 19.60(6) | 4.283(1) | | | | 202.5(2) | 3.54(4) |
| Theor. [d] | 19.799 | 4.294 | | | | 203.3 | 3.6 |
| Theor. [e] | 18.904 | 4.229 | | | | 205.7 | 3.90 |
| | | | | Zinc blende | | | |
| This work | 22.841 | 4.504 | | | | 160.8 | 5.73 |
| Expt. [g] | 24.65 | 4.62 | | | | | |
| Theor. [d] | 24.551 | 4.614 | | | | 156.8 | 3.6 |
| Theor. [e] | 22.914 | 4.508 | | | | 161.7 | 3.95 |

[a]Room-temperature x-ray-diffraction data from Ref. 24.
[b]Room-temperature EDXD data obtained using a synchrotron-radiation source from Ref. 25.
[c]Taken from Ref. 49.
[d]Hartree-Fock linear combination of atomic orbitals (LCAO) calculations from Ref. 48.
[e]LDA calculations from Ref. 9.
[f]Values extrapolated to ambient pressure and taken at room temperature.
[g]Data reported in Refs. 57 and 10.

zinc as valence electrons. We used the local-density approximation (LDA) for the exchange and correlation potential, obtained from the Monte Carlo data of Ceperly and Alder (Ref. 37) as parametrized by Perdew and Zunger (Ref. 38). The use of the LDA implies an underestimate of the band gap in semiconductors, which can be significantly improved by treating exchange and correlation within the so-called $GW$ approximation.[39–41] We have obtained, for the optimized cell of the wurtzite structure, a band gap of 0.9 eV in agreement with other similar calculations.[10] This value is much smaller than the experimental gap (3.44 eV, Ref. 42), which is correctly reproduced by the $GW$ calculations.[10,11]

As starting point for the lattice-dynamical calculations, we obtained the electronic charge density for wurtzite, zinc-blende, and rocksalt structures at different pressures, optimizing at constant pressure the lattice and the internal parameters (for the wurtzite structure). The electronic band-structure calculation was performed for the ground-state wurtzite structure using a grid of $6\times6\times3$ points for integration over the Brillouin zone (BZ),[43] and a cutoff energy of 80 hartree for the plane-wave expansion of the Kohn-Sham orbitals. For the zinc-blende and rocksalt modifications a grid of $4\times4\times4$ **k** points was employed, together with an energy cutoff of 60 hartree. These values allow a convergence of the total energy to better than 1 m hartree per unit formula. Table I displays the calculated lattice parameters and several other structural parameters for the three phases at $V_0$, the calculated equilibrium volume at zero pressure. The comparison with experimental data for the wurtzite structure shows an underestimate of the lattice constants by less than 1.6% (3.9% in volume), whereas the ratio $c/a$ is slightly overestimated (0.8%). These are typical deviations within the LDA. More elaborate density functionals, based on the generalized gradient approximation, do not improve agreement between calculations and experimental data, as shown below.

Phonon frequencies and atomic displacements were subsequently obtained using the linear-response method, which avoids the use of supercells and allows the calculation of the dynamical matrix at arbitrary **q** vectors. The force constants were extracted from a Fourier transform of the dynamical matrices obtained for a grid in the BZ. These were later employed to obtain, by interpolation, the phonon frequencies at arbitrary points in reciprocal space and the phonon-dispersion relations. The phonon frequencies were converged to better than 2 cm$^{-1}$ with the plane-wave energy cutoffs and sampling grids of **k** points mentioned above. The one- and two-phonon DOS, as well as the zinc and oxygen partial phonon DOS, were also calculated using these force constants. Technical details about the actual computation of responses to atomic displacements and homogeneous electric fields can be found in Ref. 44.

## III. STRUCTURAL PROPERTIES AND PHASE TRANSITIONS

Zinc oxide crystallizes in the wurtzite structure under normal pressure conditions.[45] However thin films can be grown in the metastable zinc-blende modification.[27,28] This behavior is related to the similarity between both structures, which differ only in the stacking of second nearest neighbors, and has been observed also in other optoelectronic materials such as AlN and GaN.[46,47] Nanocrystalline powder of rocksalt ZnO has been recently synthesized at high pressure and temperature.[29]

### A. Ground state

Table I displays the calculated lattice parameters compared to other calculations and experimental data reported in the literature.[9,24,25,48,49] For this comparison the temperature of the sample during the experiment must be taken into account. The *ab initio* calculations are usually performed with the atoms at fixed positions, whereas the experimental data of Table I correspond to room temperature, so the thermal expansion of the lattice should be considered. Even comparison with experimental data at the lowest temperatures available is, strictly speaking, not correct, since it neglects the anharmonic effect of the zero-point vibrations (see Fig. 3 of Ref. 50). *Ab initio* data should always be compared with unrenormalized experimental data for $T=0$ K, i.e., after removing the anharmonic contribution of the zero-point vibrations. This comparison usually ameliorates the discrepancies between calculated and experimental data, as it is shown in the following. Our data underestimate $a$ and $c$, measured at 300 K by energy-dispersive x-ray diffraction (EDXD),[24,25] by $\approx 1.6\%$ and 0.8%, respectively. Similar discrepancies are obtained from other LDA calculations performed with a Gaussian basis.[9] The calculations performed with the generalized gradient approximation for the exchange and correlation energy,[9] or using a Hartree-Fock approach with a linear combination of Gaussian-type orbitals,[48] tend to overestimate even the 300 K experimental data.

The deviations between LDA calculations and experimental data are already reduced, though only little, if we compare with experimental data at 4 K reported in Ref. 51 ($a=3.2483$ Å and $c=5.2035$ Å). However, if we compare our calculations with the unrenormalized values the difference is further reduced and we underestimate the lattice parameters by 1.2% and 0.5%, respectively. The bare values of $a$ and $c$, corresponding to fixed atomic positions, can be obtained by linear extrapolation of the high temperature data in Fig. 1 of Ref. 52 to $T=0$ K, following the prescription illustrated in Fig. 3 of Ref. 50. We have obtained by this procedure a renormalization of $+0.38\%$ and $+0.24\%$ for $a$ and $c$ at 0 K, respectively.[53] These values lie between those reported for diamond[54] and Ge,[55] $+0.37\%$ and $+0.18\%$, respectively. The unrenormalized $a$ and $c$ agree somewhat better with the calculated (LDA) results than the renormalized values obtained directly from experiments.

We discuss next the bulk modulus $B_0$. We should, in principle, also take into account the temperature dependence of $B_0$ in a similar way as we have done for the lattice parameters, using the linear extrapolation procedure discussed above. We find from Ref. 56 that the unrenormalized elastic stiffness constants are $\approx 2\%$ larger than the room-temperature values. Taking for comparison the data at 300 K from Ref. 25, which have the smallest error bars of all available experimental data, and correcting for the difference between 300 K and 0 K, the vibrational renormalization correction allows us to reduce the discrepancy between our calculations and the experimental results to 9.7%. The renormalization of the bulk modulus is not negligible even at 0 K, where it amounts to 1.1%.

The experimental lattice parameters for the rocksalt structure displayed in Table I result from a fit of the pressure dependent EDXD data extrapolated to ambient pressure. Unfortunately, no information is available on the thermal expansion for this phase, and we can compare our calculations only with room-temperature data. The calculated lattice constant is also smaller than the experimental values, presumably due to the reasons discussed above for the wurtzite modification. It is not possible to infer how much of the discrepancy in Table I for the rocksalt structure is due to errors in the local-density approximation. However, LDA calculations performed by Jaffe *et al.*[48] report similar values of the lattice constant. The bulk modulus of 209.1 GPa is in line with data obtained using EDXD under pressure with a synchrotron-radiation source and with other theoretical values listed in Table I.

There are very few reports of the existence of the zinc-blende ZnO phase at ambient conditions.[10,28,57] To the best of our knowledge, the only experimental result is the lattice constant $a=4.62$ Å.[57] This value is 2.5% larger than that obtained from our calculations which, in turn, is similar to the value reported in Ref. 9. This discrepancy would also be reduced if we take into account a vibrational renormalization similar to that used for the wurtzite modification. Our value of $B_0$ for zinc blende lies between those reported in other theoretical papers, although we obtain a larger value for its pressure derivative, $B'$.

### B. Phase transitions

Wurtzite-ZnO undergoes a phase transition to the rocksalt modification upon application of pressure.[26] This transition has been observed by EDXD using conventional sources[24] as well as synchrotron radiation,[25] yielding a transition pressure of 8.7(5) and 9.1(2) GPa, respectively. In Table II we compare these values with those obtained from our and other *ab initio* calculations. However, Refs. 24 and 25 report a strong hysteresis in the transition of up to 6 GPa, the rs$\rightarrow$wz transition being complete only at 2 GPa when lowering the pressure. The wz$\rightarrow$rs transition occurs due to the instability of the wurtzite structure against a shearing deformation, which has been recently reported in ultrasonic experiments under pressure[58] and confirmed by theoretical calculations.[59] This mechanism has also been proposed for the wurtzite-to-rocksalt transformation of GaN.[60] The wurtzite-to-rocksalt transition also presents a pressure range where both phases coexist, between 9.1 and 9.6 GPa according to Ref. 25 and between 10 and 15 GPa according to Ref. 61. This last ref-

TABLE II. Transition pressure $p_t$ and relative volume change $\Delta V_t/V_t^{wz}$ at the structural transition from the wurtzite to the NaCl modification.

| | $p_t$ | $\Delta V_t/V_t^{wz}$ (%) |
|---|---|---|
| This work | 10.1 | 16 |
| Expt. [a] | 8.7(5) | 17.5 |
| Expt. [b] | 9.1(2) | 15.5 |
| Theor. [c] | 8.57 | 18.4 |
| Theor. [d] | 6.60 | 16.7 |

[a]X-ray-diffraction data from Ref. 24.
[b]Energy-dispersive x-ray-diffraction data using a synchrotron-radiation source reported in Ref. 25.
[c]Hartree-Fock LCAO calculations from Ref. 48.
[d]LDA calculations from Ref. 9.

erence also reports metastability of the rocksalt phase at 1 bar after decompression, which has been applied to produce nanocrystallites of rocksalt-ZnO in a high-pressure cycle.[29] The origin of the disagreement in the transition pressure between both data sets is not clear, since in both cases EDXD data were taken using synchrotron radiation as x-ray source. Calculations performed using a Hartree-Fock formalism yield values of the transition pressure [8.57 and 6.60 GPa (Ref. 62)] that lie below the experimental results, whereas the results of our calculations (10.1 GPa) lie in the range of the experimental values. The relative change of volume at the transition pressure, however, is correctly described by the mentioned theoretical results as well as our calculations. Jaffe *et al.*[9] have predicted an additional transition from the rocksalt to the CsCl structure at around 260 GPa. The highest pressure which has been reached in the EDXS experiments is 56(1) GPa.[25]

## IV. LATTICE DYNAMICS AND ITS PRESSURE DEPENDENCE

### A. Phonon frequencies and eigenvectors

#### *1. Wurtzite*

We have listed in Table III our calculated frequencies of the phonons at the center of the BZ for ZnO in the wurtzite structure at the theoretical zero-pressure volume $V_0$. We also list their calculated eigenvectors, the first and second derivatives of the frequencies vs pressure and the corresponding Grüneisen parameters, including measurements at 7 K performed by us (see Ref. 63 for experimental details). The experimental frequencies are also affected, even at low temperatures, by anharmonic and isotopic renormalization.[64,65] The latter affects mainly the high-frequency phonons and would be due to the oxygen mass fluctuations which are basically negligible for natural oxygen (99.8% $^{16}$O). The anharmonic renormalization can be obtained, for the $E_2^{high}$ phonons, from available data for their temperature dependence:[20] It amounts to $-5$ cm$^{-1}$. Subtracting this number to the measured frequency of 438 cm$^{-1}$, we obtain 443 cm$^{-1}$ which is only 0.7% larger than our calculated value. If we assume a similar renormalization for the $E_1^{TO}$ and $A_1^{TO}$ frequencies, we find a difference of 1%–2% with our calculations. The measured LO frequencies are about 7% higher than the calculated ones. This difference correlates with the difference between calculated and experimental values of $\epsilon_\infty$ (see Table IV), to be discussed below. The computer code calculates the LO frequency using the expression [see Eq. (63) of Ref. 44]

$$\omega_{LO}^2=\omega_{TO}^2+\frac{4\pi Z^{*2}}{V_0\mu\epsilon_\infty}, \tag{1}$$

where $Z^*$ is the transverse effective charge, and $V_0$ and $\mu$ the volume and reduced mass per unit formula, respectively.

TABLE III. Calculated phonon frequencies $\omega$, phonon eigenvectors $e_{Zn}$ and $e_O$, and their pressure dependence at the $\Gamma$ point for the wurtzite structure. Frequencies are given in cm$^{-1}$ and their pressure coefficients in cm$^{-1}$/GPa and cm$^{-1}$/GPa$^2$. Experimental data are given in parentheses. The calculated Grüneisen parameters have been obtained using a bulk modulus of 159.5 GPa. The sign of the eigenvectors specifies the relative displacement of the oxygen atom located on top of the zinc atom along the *c* axis. The eigenvector normalization corresponds to four atoms per primitive cell.

| | $\omega$ | $e_{Zn}$ | $e_O$ | $\frac{\partial\omega}{\partial p}$ | $\frac{\partial^2\omega}{\partial p^2}$ | $\gamma$ |
|---|---|---|---|---|---|---|
| $E_2^{low}$ | 91 (100 [a]) | 0.653 | $-0.272$ | $-1.05$ ($-0.85$ [b], $-0.93$ [c]) | $-0.027$ | $-1.86$ ($-1.21$ [b],$-1.6$ [c]) |
| $B_1^{low}$ | 261 | 0.701 | 0.096 | 1.50 | $-0.041$ | 0.92 |
| $A_1^{TO}$ | 391 (380 [a], 379 [b]) | 0.309 | $-0.636$ | 5.29 (4.33 [b], 4.72 [c]) | $-0.093$ | 2.16 (1.63 [b], 2.1 [c]) |
| $E_1^{TO}$ | 409 (410 [a], 411 [b]) | 0.314 | $-0.634$ | 5.22 (5.2 [b], 4.38 [c]) | $-0.096$ | 2.04 (1.80 [b, c]) |
| $E_2^{high}$ | 440 (438 [a], 439 [b, c]) | 0.272 | 0.653 | 5.58 (5.11 [b], 5.16 [c]) | $-0.101$ | 2.02 (1.66 [b],2.0 [c]) |
| $B_1^{high}$ | 552 | 0.096 | $-0.701$ | 4.96 | $-0.073$ | 1.43 |
| $A_1^{LO}$ | 560 (584 [a], 575 [b, c]) | 0.309 | $-0.636$ | 4.77 (4.75 [b]) | $-0.089$ | 1.37 (1.17 [b]) |
| $E_1^{LO}$ | 556 (595 [a], 580 [c], 588 [d]) | 0.314 | $-0.634$ | 4.39 (4.77 [c]) | $-0.071$ | 1.24 (1.4 [c]) |

[a]Our Raman data for natural ZnO at 7 K.
[b]Raman data for natural ZnO at room temperature (Ref. 22), $B_0=143$ GPa.
[c]Raman data for natural ZnO at room temperature (Ref. 21), $B_0=170$ GPa.
[d]Raman data for natural ZnO at room temperature (Ref. 51).

TABLE IV. Pressure dependence of the Born effective charges $Z^*$ of the ir-active modes of ZnO and the dielectric constants in the wurtzite (wz), zinc-blende (zb), and rocksalt (rs) structures. For the wurtzite structure, the upper and lower rows correspond to $E_1$ and $A_1$ modes, respectively. Experimental data are shown in parentheses and results from other calculations are shown in brackets.

| Phase | $Z^*(e)$ | $\frac{\partial Z^*}{\partial p}(\times 10^{-3}\ e/\mathrm{GPa})$ | $\epsilon_\infty$ | $\frac{\partial \epsilon_\infty}{\partial p}(\times 10^{-3}\ \mathrm{GPa}^{-1})$ |
|---|---|---|---|---|
| | $\perp$ 2.14 (2.16[a]) | −3.0 | 5.36 (4.11[b]) | −18 (−14[b]) |
| wz | $\|\|$2.11 (2.22[a])[2.05[c], 2.11[d]] | −2.8 | 4.47 (4.03[b]) | −6 (−14[b]) |
| zb | 2.13 | −3.1 | 5.10 | −14 |
| rs | 2.45 | −2.2 | 5.44 | −17 |

[a]Our Raman data, measured at 7 K. The only experimental data for $Z^*$ found in the literature is 2.09 (Ref. 82); it was obtained by taking a weighted average of the squares of the TO and LO phonon frequencies for the $A_1$ and $E_1$ modes (Ref. 83).
[b]Derived from the refractive indices given in Ref. 71.
[c]*Ab initio* calculations from Ref. 84.
[d]*Ab initio* calculations from Ref. 85.

$Z^*$ is obtained by evaluation of the effect of an electric field without using the incorrect calculated values of $\epsilon_\infty$.

Among the calculated eigenvectors listed in Table III, those of the $A_1$ and $E_1$ modes can be obtained simply by invoking the conservation of the center of mass, since there is only one set of phonons of each symmetry. This procedure leads for the $A_1$ and $E_1$ eigenvectors to $e_{\mathrm{Zn}}=0.314$ and $e_{\mathrm{O}}=-0.634$, in perfect agreement with the listing for $E_1^{\mathrm{TO}}$ and $E_1^{\mathrm{LO}}$ in Table III. The slight difference found in this table for $A_1^{\mathrm{TO}}$ and $E_1^{\mathrm{TO}}$ ($\approx 1\%$) gives an indication of the computational accuracy. The $B_1$ and $E_2$ eigenvectors are not fixed by symmetry since there are two of each kind. However, because of orthonormality, each depends only on one free parameter. No experimental data are available for the $B_1$ eigenvectors which, according to the calculations, turn out to be nearly pure oxygen-like and zinc-like. The $E_2$ eigenvectors have also been determined from the dependence of their frequencies on isotope masses.[63] They are $|e_{\mathrm{O}}|=0.65(1)$ and $|e_{\mathrm{Zn}}|=0.27(1)$, also in excellent agreement with the calculated values.

The calculated $\partial\omega/\partial p$ show the usual trends found for wurtzite and zinc-blende-type semiconductors: The $E_2^{\mathrm{low}}$ phonons, equivalent to the TA(L) modes of zinc blende, have a negative derivative whereas all others are positive. Moreover, $\partial\omega/\partial p$ is larger for the TO modes than for the LO modes, a fact which has been interpreted as reflecting a decrease in ionicity with increasing pressure (exception SiC, see Ref. 66). The calculated negative values of $\partial^2\omega/\partial p^2$ indicate that the pressure dependence of the corresponding frequencies is sublinear for all modes except for $E_2^{\mathrm{low}}$, in agreement with other materials of the family (see Ref. 67 for GaP and Si). The experimental values of the mode Grüneisen parameters $\gamma$ are in good agreement with the calculated ones and also reflect the trends discussed for $\partial\omega/\partial p$. A large discrepancy between measured and calculated $\gamma$'s is found for the LO modes. This may result from experimental inaccuracies related to the rather broad $E_1^{\mathrm{LO}}$ Raman spectrum displayed in Fig. 1 of Ref. 21. The calculation of the thermal expansion is not as easy as it may seem except for the material with the zinc-blende structure for which no experimental data are available. It would indeed be quite interesting to calculate the expansion along $a$ and $c$ for the wurtzite structure for which, as mention in the text, extensive data are available.[52] In this case the thermal expansion along $a$ and $c$ are different and, in order to evaluate them, it does not suffice to use the volume Grüneisen parameters but one must use the dependence of all phonon frequencies on strain along $a$ and $c$.[68] This requires considerable computational effort and must be left for future work. Even for the cubic case it is not clear how large a sampling of Grüneisen parameters will be required to obtain reliable $V(T)$ curves. This will be investigated when the wurtzite calculation is undertaken.

Table IV also shows excellent agreement between experimental and calculated values of $Z^*$. The agreement is not as satisfactory for $\epsilon_\infty$: The fact that the calculated $\epsilon_\infty^{\|,\perp}$ are larger than the measured ones can be attributed to the LDA gap problem which has been already mentioned in Sec. II. The electronic contribution to the susceptibility is known to increase with decreasing average gap, the so-called Penn gap $E_{\mathrm{Penn}}$,[69] which usually corresponds to the gap at the X point of the zinc-blende structure. Using Penn's expression

$$\epsilon_\infty - 1 = \frac{E_p^2}{E_{\mathrm{Penn}}^2}, \tag{2}$$

where $E_p$ is the plasma energy of the valence electrons, we find, after correction for the gap problem for the closely related ZnS (with zinc-blende structure, Ref. 70, the situation should be very similar for wurtzite ZnO), a decrease in $\epsilon_\infty - 1$ by a factor of 0.6 which overcorrects the discrepancy in $\epsilon_\infty - 1$ shown in Table IV (a decrease by a factor of 0.8). In spite of this discrepancy, the average of the calculated $\partial\epsilon_\infty^{\|}/\partial p$ and $\partial\epsilon_\infty^{\perp}/\partial p$, $\partial\langle\epsilon_\infty\rangle/\partial p = -13\times 10^{-3}\ \mathrm{GPa}^{-1}$, agrees rather well with the experimental value $(-14\times 10^{-3}\ \mathrm{GPa}^{-1})$.[71]

Table V lists the "Grüneisen parameters," i.e., the logarithmic derivatives vs volume with the sign reversed, of $\epsilon_\infty$ ($\gamma_\infty$) and $Z^*$ ($\gamma^*$). The calculated $\gamma^*$ is obtained directly from the calculated $Z^*$ vs volume, whereas the experimental one is obtained with the expression

TABLE V. Comparison between experimental data and calculated Grüneisen parameter $\gamma_\infty$ of the dielectric constants and those of the Born effective charges $\gamma^*$ for the wurtzite structure, derived from the data listed in Table IV.

| | $\gamma_\infty$ | | $\gamma^*$ | |
|---|---|---|---|---|
| | $\parallel$ | $\perp$ | $\parallel$ | $\perp$ |
| This work | −0.21 | −0.54 | −0.21 | −0.22 |
| Expt. [a] | −0.48 | −0.50 | −0.21 | +0.21 [b] |

[a]The refractive indices were taken from Ref. 71, the phonon frequencies and Grüneisen parameters from Table III.

[b]Experimental data from Ref. 21. The LO phonons may have a slight plasmon component which broadens the Raman peak and possibly vitiates the value of $\gamma_{LO}$ (see text).

$$\gamma^* = \gamma_{\mathrm{LO}} + \frac{(\gamma_{\mathrm{LO}} - \gamma_{\mathrm{TO}})\omega_{\mathrm{TO}}^2}{\omega_{\mathrm{LO}}^2 - \omega_{\mathrm{TO}}^2} + \frac{1}{2}\gamma_\infty - \frac{1}{2}, \qquad (3)$$

derived from Eq. (1). Whereas for the polarization parallel to the *c* axis experimental and calculated data are in perfect agreement, this is not the case for the perpendicular polarization. As already mentioned, we believe that the reason may lie in an inaccurate experimental value of $\gamma_{\mathrm{LO}}(E_1)$ due to the broad and weak spectral feature for which this determination was made.[21] The calculated negative sign of $\gamma^*$ agrees with that found for all zinc-blende-type semiconductors with the exception of SiC.[66] For GaN, an isoelectronic material with wurtzite structure, we find from the data in Ref. 72 $\gamma^* = -0.10(5)$.

Table VI displays the phonon frequencies, their pressure coefficients, and Grüneisen parameters for A (0 0 0.5), H (1/3 1/3 0.5), and L (0.5 0 0.5), high-symmetry points of the BZ of the wurtzite structure. We have selected these points as representative of the edge of the BZ because they present the largest degeneracy of the phonon frequencies. Similar to the case of the phonons at Γ, the Grüneisen parameters for TO modes are significantly larger than those corresponding to LO phonons. The other trends discussed for the Γ phonons also apply here; namely, the low-frequency phonons, related to the TA modes at the zone edge of the zinc-blende structure, exhibit a negative Grüneisen parameter. We may conjecture that this behavior should be found throughout most of the boundary of the BZ, since the phonons at A are the lowest-lying modes at this boundary. This is corroborated by experimental data for the temperature dependence of the linear thermal-expansion coefficient $\alpha(T)$, which can be expressed as a sum of Grüneisen parameters weighted by Bose-Einstein factors.[73] The low-frequency modes dominate at low temperature, a fact that yields a sign reversal in $\alpha(T)$, which is negative at low *T* due to the contribution of $\gamma_{\mathrm{TA}}$ at the zone edge, and becomes positive with the activation of LA and optic phonons at higher temperature. At even lower temperatures, for the group IV and III-V semiconductors, the expansion coefficient may experience an additional change of sign and become slightly positive, due to the contribution of the positive Grüneisen parameters of the elastic constants. This has been explained in detail in Ref. 73, where first-principles calculations show two changes of sign for GaAs but just one for ZnSe. For this material the Grüneisen parameters of the elastic constants are also negative. For ZnO, only a sign reversal has been reported[51] for $\alpha(T)$, a fact possibly related to the already negative value for the Grüneisen parameter of the TA(A) modes. These modes correspond to folded Λ modes of zinc blende (see the following section) and should reflect the sign of the Grüneisen parameters of the elastic constants.

TABLE VI. Phonon frequencies (in $\mathrm{cm}^{-1}$), pressure coefficients (in $\mathrm{cm}^{-1}/\mathrm{GPa}$ and $\mathrm{cm}^{-1}/\mathrm{GPa}^2$) and Grüneisen parameters of several modes for the wurtzite structure at certain high-symmetry points of the Brillouin zone. For the Grüneisen parameter calculation we have used $B_0 = 159.5$ GPa.

| | $\omega$ | $\frac{\partial\omega}{\partial p}$ | $\frac{\partial^2\omega}{\partial p^2}$ | $\gamma$ |
|---|---|---|---|---|
| A | 69 | −0.84 | −0.002 | −1.96 |
| | 189 | 1.30 | −0.027 | 1.10 |
| | 424 | 5.40 | −0.095 | 2.03 |
| | 557 | 4.56 | −0.064 | 1.31 |
| H | 99 | −1.25 | −0.030 | −2.01 |
| | 165 | −0.18 | −0.034 | −0.17 |
| | 258 | 1.89 | −0.034 | 1.17 |
| | 454 | 5.59 | −0.089 | 1.96 |
| | 514 | 5.45 | −0.080 | 1.69 |
| | 539 | 4.77 | −0.072 | 1.41 |
| L | 111 | −0.88 | −0.024 | −1.26 |
| | 115 | −1.00 | −0.025 | −1.39 |
| | 267 | 1.78 | −0.036 | 1.06 |
| | 465 | 5.43 | −0.082 | 1.86 |
| | 467 | 5.60 | −0.093 | 1.91 |
| | 554 | 4.81 | −0.069 | 1.38 |

### *2. Zinc blende and rocksalt*

The phonon frequencies of several high-symmetry points for the zinc-blende structure, as well as their dependence on pressure, are displayed in Table VII. As we discussed in Sec. III, wurtzite and zinc-blende modifications show the same atomic surrounding for the first nearest neighbors. Whereas wurtzite has a sublattice stacking ABABAB . . . along the *c* axis, zinc blende shows a different stacking ABCABC . . . , this time along the ⟨111⟩ direction. This, and the fact that the wurtzite primitive cell has four atoms along the *c* axis, allows us to consider the phonon-dispersion relations of the wurtzite structure along Γ-A as backfolded from those of Γ-L in the zinc-blende BZ. This explains the similarity between the frequencies obtained for the TA and TO modes at L and those of the $E_2^{\mathrm{low}}$ and $E_2^{\mathrm{high}}$ at Γ, similarity which is even carried over to their pressure dependence. For example, for TO(L) we obtain a phonon frequency of 443 $\mathrm{cm}^{-1}$ and a Grüneisen parameter of 1.99, whereas its equivalent mode in the wurtzite structure, with $E_2^{\mathrm{high}}(\Gamma)$ symmetry, was calculated to be at 440 $\mathrm{cm}^{-1}$ and its Grüneisen parameter 2.02.

Table VIII lists the phonon frequencies and their pressure

TABLE VII. Phonon frequencies (in $cm^{-1}$), pressure coefficients (in $cm^{-1}$/GPa and $cm^{-1}$/$GPa^2$), and Grüneisen parameters of several modes for the zinc-blende structure at certain high-symmetry points of the Brillouin zone. For the Grüneisen parameter calculation we have used $B_0 = 160.8$ GPa.

| | | $\omega$ | $\frac{\partial\omega}{\partial p}$ | $\frac{\partial^2\omega}{\partial p^2}$ | $\gamma$ |
|---|---|---|---|---|---|
| Γ | TO | 403 | 5.15 | −0.084 | 2.03 |
| | LO | 558 | 4.55 | −0.072 | 1.31 |
| X | TA | 128 | −0.99 | −0.044 | −1.24 |
| | LA | 269 | 1.98 | −0.032 | 1.18 |
| | TO | 487 | 5.61 | −0.088 | 1.85 |
| | LO | 551 | 4.70 | −0.056 | 1.37 |
| L | TA | 93 | −0.99 | −0.032 | −1.71 |
| | LA | 264 | 1.45 | −0.036 | 0.88 |
| | TO | 443 | 5.48 | −0.092 | 1.99 |
| | LO | 561 | 4.94 | −0.072 | 1.42 |

dependence for the rocksalt structure, calculated at the equilibrium volume $V_0$. In order to facilitate comparison with future experiments, we give also the Grüneisen parameters at 8 GPa for the Γ phonons, i.e., at a pressure close to the transition from the wurtzite structure. The most significant aspect of these data is the positive value of all Grüneisen parameters listed in Table VIII. This, according to the arguments mentioned above, would yield a positive linear thermal-expansion coefficient at all temperatures for rocksalt-type ZnO. To the best of our knowledge, the only data available in the literature for Grüneisen parameters of crystals with the rocksalt structure are those reported for Rb halides.[74,75] These data yield negative values for the TA(X) and LA(X) phonons of RbBr, of the order of $-0.50$,[75] and also, but larger in magnitude, for RbI.[74] Measurements of the phonon-dispersion relations under pressure performed recently[76] on PbTe have yielded a very small but negative value of $\gamma_{TA}$ for the X point, contrary to our calculations for ZnO. In contrast to calculations reported for GaP,[77] the rocksalt structure of ZnO exhibits a very small but positive Grüneisen parameter for the TA(X) mode, as shown in Table VIII. This behavior may be related to the nonmetallic nature of the rocksalt modification of ZnO, which is deduced indirectly from the nonzero LO-TO splitting at the Γ point and has been recently observed in measurements of the optical absorption, and also obtained in *ab initio* calculations.[78] GaP seems to be metallic in the rocksalt structure.[77]

TABLE VIII. Phonon frequencies (in $cm^{-1}$), pressure coefficients (in $cm^{-1}$/GPa and $cm^{-1}$/$GPa^2$), and Grüneisen parameters of several modes for the rocksalt structure at certain high-symmetry points of the Brillouin zone. For the Grüneisen parameter calculation we have used $B_0 = 209.1$ GPa.

| | | $\omega$ | $\frac{\partial\omega}{\partial p}$ | $\frac{\partial^2\omega}{\partial p^2}$ | $\gamma$ |
|---|---|---|---|---|---|
| Γ | TO | 235 | 5.14 | −0.106 | 4.57 [a] |
| | LO | 528 | 3.68 | −0.056 | 1.29 [b] |
| X | TA | 138 | 0.56 | −0.038 | 0.85 |
| | LA | 215 | 1.35 | −0.054 | 1.31 |
| | TO | 353 | 4.42 | −0.068 | 2.62 |
| | LO | 462 | 4.07 | −0.046 | 1.84 |
| L | TA | 135 | 1.82 | −0.026 | 2.82 |
| | LA | 298 | 1.33 | 0.036 | 0.93 |
| | TO | 201 | 6.22 | −0.252 | 6.47 |
| | LO | 519 | 3.61 | −0.050 | 1.45 |

[a]The Grüneisen parameter at 8 GPa is 4.24.

[b]The Grüneisen parameter at 8 GPa is 1.51.

According to Table IV, the calculated values of $\partial Z^*/\partial p$ are rather similar for the three ZnO modifications. This derivative can be related to the derivative of an effective charge with respect to the bond length.[66] Because of the similarity of the bonds in the wurtzite and zinc-blende structures, it is not surprising to find similar values of $\partial Z^*/\partial p$ (and also $\partial\epsilon_\infty/\partial p$) for both structures. It is not so obvious that the rocksalt modification should behave in the same way. $\partial Z^*/\partial p$, if related to the derivative of $Z^*$ with respect to a bond length, can be estimated to be somewhat smaller for rocksalt than that for the zinc-blende and wurtzite structures, in agreement with the predictions in Table IV. The fact that $\partial\epsilon_\infty/\partial p$ is also similar for the three modifications reflects the fact that $E_{\mathrm{Penn}}$, in the denominator of Eq. (1), increases with increasing pressure sufficiently to overcompensate the effect of the increase of $E_p$, which appears in the numerator of that equation.

Figure 1 displays the calculated phonon-dispersion relations for the three phases investigated at the volume $V_0$ defined in Table I. The solid diamonds are Raman data for the wurtzite structure,[63] whereas the open and solid circles represent INS data from Refs. 13 and 15, respectively. For the rocksalt structure, Fig. 1(c) shows also the dispersion relations calculated at 8 GPa, i.e., close to the phase transition (thick curves). On the right-hand side of the graphs we plot the one-phonon DOS [solid curve, $\rho^{(1)}(\omega)$] and the zinc and oxygen partial phonon DOS, displayed by dashed and dotted lines, respectively. These densities of states can be used for calculating the renormalization of phonon frequencies and linewidths due to isotopic mass disorder. This renormalization is given, for the zinc-blende structure, by[79]

$$\Gamma_{\mathrm{iso}} = \frac{\pi}{6}\omega^2\left(g_2^{\mathrm{O}}\rho_{\mathrm{O}}^{(1)}(\omega)|e_{\mathrm{O}}(\omega)|^2 + g_2^{\mathrm{Zn}}\rho_{\mathrm{Zn}}^{(1)}(\omega)|e_{\mathrm{Zn}}(\omega)|^2\right), \tag{4}$$

where $\rho_{\mathrm{O,Zn}}^{(1)}$ are the one-phonon DOS projected on the oxygen and zinc sublattices (normalized to 3), $g_2^{\mathrm{O,Zn}}$ are the mass variance parameters of the oxygen and zinc sublattices,[79] and the eigenvectors are normalized to make the sum of the squares equal to one. For natural ZnO $g_2^{\mathrm{O}} \approx 0$. For the $E_2^{\mathrm{low}}$ modes we obtain, using Eq. (4) and $\rho_{\mathrm{Zn}}^{(1)}$ of Fig. 1(a), for natural ZnO ($g_2^{\mathrm{Zn}} = 6\times10^{-4}$) an isotopic broadening of 0.06 $cm^{-1}$. A value of less than 0.1 $cm^{-1}$ has been reported in the literature[63] for the total width of this mode at 7 K. Hence, most of the measured width must be due to isotopic disorder. For $^{64}Zn_{0.5}^{68}Zn_{0.5}$ ($g_2^{\mathrm{Zn}} = 9\times10^{-4}$), for which crystals are available,[63] the isotopic disorder-induced broadening

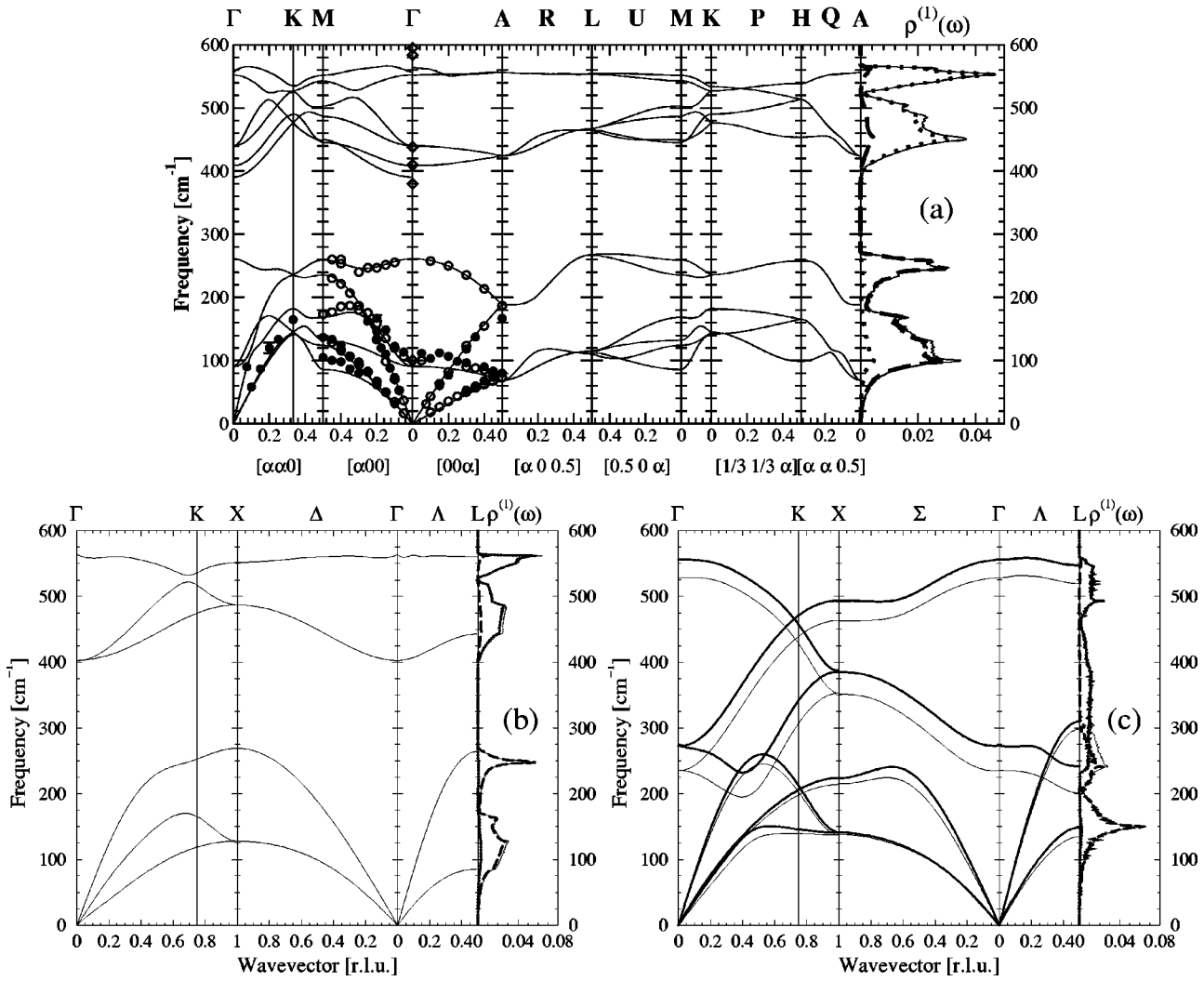


FIG. 1. Phonon-dispersion relations and one-phonon DOS $[\rho_1(\omega)]$ of (a) wz, (b) zb, and (c) rs phases, calculated at the equilibrium volume (zero pressure and temperature, thin lines) given in Table I. The thick lines in (c) display the dispersion relations of the rocksalt phase at 8 GPa, i.e., close to the phase transition. On the right-hand plots, the solid curves represent the one-phonon DOS, whereas dashed and dotted curves display the projected DOS corresponding to zinc and oxygen displacements, respectively. The diamonds stand for Raman data reported in Ref. 63 whereas the solid and open circles display INS data of Refs. 13 and 15.

should amount to 0.09 $cm^{-1}$. We have obtained for the $E_2^{high}$ phonons a renormalization of the phonon linewidth of 5 $cm^{-1}$ (full width at half maximum, FWHM) for $^{nat}Zn^{16}O^{18}_{0.5}O_{0.5}$, in reasonable agreement with the experimental value of 7 $cm^{-1}$ reported in Ref. 32.

The few INS data available for the dispersion relations of wurtzite in the 240–260 $cm^{-1}$ region agree very well with the calculations. The position of the corresponding peak in $\rho^{(1)}(\omega)$ (250 $cm^{-1}$) should therefore be given rather reliably in $\rho^{(1)}(\omega)$ of Fig. 1(a). Good agreement is also obtained for the linear parts of the acoustic dispersion relations. This is not the case for most of the other INS data shown in Fig. 1(a). For instance, the measured lower TA modes at *M* lie 20% higher than the calculated ones. As already displayed in Table III, the measured $E_2^{low}$ frequency is 10% larger than the calculated value. We have already compared the higher Raman frequencies with the calculations in connection with Tables III and IV. $\rho^{(1)}(\omega)$ in Fig. 1(a) shows a gap which separates oxygen-like from zinc-like vibrations. The modes above the gap contain only 15% of the squared vibrational amplitude of zinc (85% of oxygen). The opposite is true for the modes below the gap. Similar behavior is shown by the zinc-blende data, in Fig. 1(b). However, no gap appears in the DOS of the rocksalt phase, a fact which is shared by PbS, PbSe, PbTe, SnTe, AgCl, and AgBr. Some of the alkali halides, however, show a gap (e.g., NaBr and NaI) while others do not (e.g., NaCl and KF).

### B. Two-phonon DOS and second-order Raman scattering

#### *1. Wurtzite*

Figure 2 displays the two-phonon sum $[\rho_+^{(2)}(\omega)]$ and difference $[\rho_-^{(2)}(\omega)]$ DOS for ZnO in the wurtzite structure at several pressures. We have tried to correlate the most salient features of the zero pressure $\rho_+^{(2)}(\omega)$ and $\rho_-^{(2)}(\omega)$ with structure seen in the second-order Raman spectra.[16,18,22] The re-

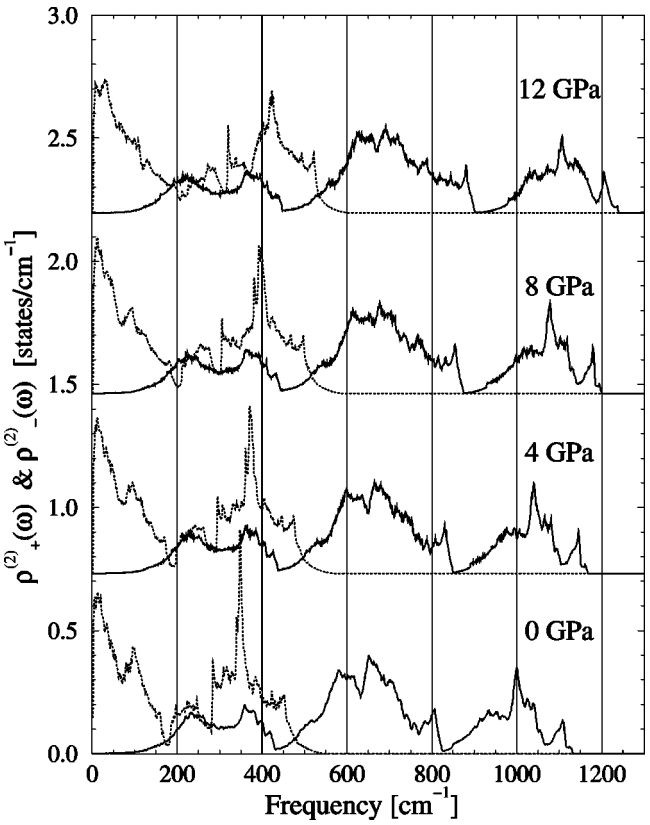


FIG. 2. Calculated two-phonon densities of states corresponding to sums (solid curves) and differences (dotted curves) of two phonons, for the wurtzite structure at several pressures. The vertical lines are guides to the eye to emphasize the pressure shifts of critical points. With the exception of the bands below $\approx$300 cm$^{-1}$, all peaks shift up with increasing pressure.

sults of this effect are described in Table IX. This table reflects the trend mentioned when comparing the calculated with the INS dispersion relations of Fig. 1(a). Most of the calculated structures lie between 5% and 10% lower than the measured ones, with the exception of the $B_1+\mathrm{LO}$ structure for which there is good agreement between calculated and experimental results. This reflects, at least in part, the rather good agreement obtained by INS for the $B_1$ branch. It is interesting to note that for the structure assigned in Table IX to $2\mathrm{TA_L}$ modes the calculated frequency lies above the experimental one. Because of the lack of INS data in the TA(L) region it is not possible to speculate about the reason for this discrepancy.

The most prominent peak in $\rho^{(2)}_-(\omega)$ in Fig. 2 lies around 348 cm$^{-1}$ at zero pressure. A prominent peak is also seen at 330 cm$^{-1}$ in the Raman spectrum and can be unambiguously assigned to difference modes because it disappears at low temperatures. It has already been assigned to TO$-$TA phonon differences.[80] The fact that the calculated peak lies well above the measured one reflects the mentioned 20% error for the TA modes ($\approx$20 cm$^{-1}$): the INS data are higher than the calculated ones; this results in the opposite effect for TO-TA.

The features in the DOS of Fig. 2 above 400 cm$^{-1}$ shift up with pressure as corresponds to dominant positive $\gamma$'s of the two constituent phonons. The features in $\rho^{(2)}_+(\omega)$ at $\approx$380 cm$^{-1}$ do not shift appreciably with pressure. They correspond to sums of LA and TA modes whose pressure shift cancel each other. The peak at 230 cm$^{-1}$ shifts down with pressure thus reflecting the negative Grüneisen parameter of the TA modes (see Table IV).

Figure 3 shows the pressure dependence of the second-order Raman spectra of $^{64}Zn^{18}O$, isotopically pure crystals used in Ref. 32, in the region where difference modes have been identified. The most prominent feature (TO$-E_2^{\mathrm{low}}$) shifts strongly with pressure[22,80] thus reflecting the positive $\gamma$ of the TO and the negative one of the TA modes. With increasing pressure this mode acquires a low-frequency shoulder which can also be identified as a difference mode by comparison with Fig. 2. It corresponds to LO$-B_1$ differences for which, on the basis of the dispersion relations of Fig. 1(a) and of Table VI, the two constituent phonons

TABLE IX. Comparison of structures in the two-phonon DOS (sum and difference modes) with second-order Raman data. The calculated and experimental (Ref. 22) pressure derivatives are given in parentheses.

| Mode | Our calculations [cm$^{-1}$ (cm$^{-1}$/GPa)] | Experiments [cm$^{-1}$ (cm$^{-1}$/GPa)] |
|---|---|---|
| $2\mathrm{LO}_\Gamma$ | 1120 (8.8) | 1200 [a, b] |
| $2\mathrm{LO}_{\mathrm{A,L,M}}$ | 1100 (8.3) | 1149 [a], 1160 [b] |
| $[\mathrm{TO}+\mathrm{LO}]_{\mathrm{A,L,M}}$ | 1000 (9.7) | 1084 [a], 1080 [b] |
| $2\mathrm{TO}_{\mathrm{A,L,M}}$ | 930 (11.3) | 986 [a], 990 [b] |
| $B_1+\mathrm{LO}$ | 810 (5.9) | 800–820 [a], 810 [b] |
| TA+LO | 650 (3.7) | 675 [a], 680 [b] |
| $[\mathrm{TA}+\mathrm{TO}]_{\mathrm{A,L,M}}$ | 590 (4.5) | overlap with first order |
| $[2B_1]_{\Gamma,\mathrm{L,M}}$ | 520 (3.0) | 540 [a], 530 [b] |
| TO$-E_2^{\mathrm{low}}$ | 348 (6.6) | 334 [a], 330 [b], 331 [c] (5.8) |
| LO$-B_1$ | 290 (3.0) | 302 [d] (3.0) [d] |
| $2\mathrm{TA_L}$ | 225 ($-$2.1) | 208 [a], 205 [b], 213 [c] ($-$3.9) |

[a]Raman data at room temperature from Ref. 16.

[b]Raman data at room temperature from Ref. 18.

[c]Raman data at room temperature from Ref. 22.

[d]Our Raman data under pressure at room temperature for $^{64}Zn^{18}O$, from Fig. 3.

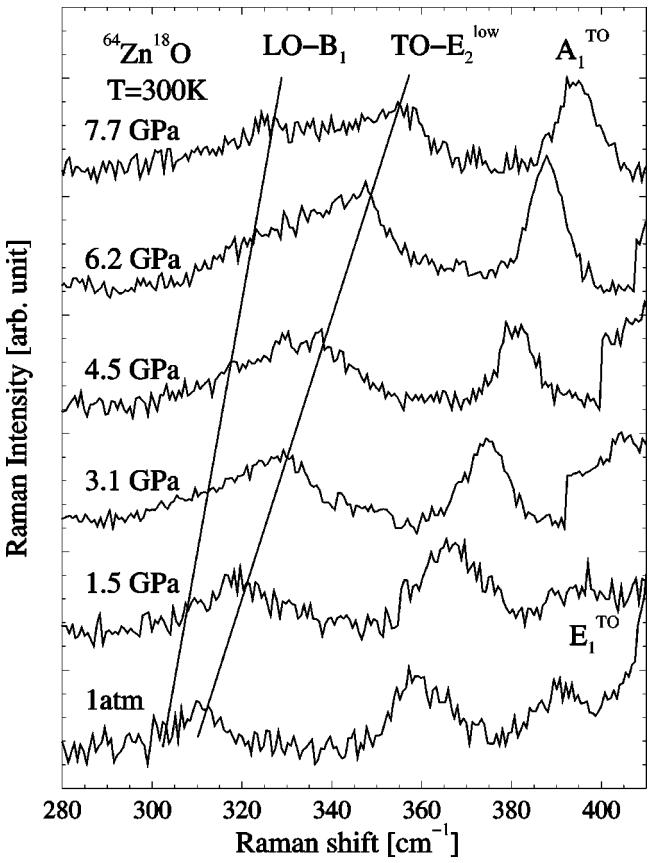


FIG. 3. Pressure dependence of the Raman spectrum of $^{64}Zn^{18}O$, showing a difference mode that corresponds to TO $-E_2^{\mathrm{low}}$ mode in the vicinity of the $M$ point of the Brillouin zone. The structure that appears at the low-frequency side is assigned to LO$-B_1$ differences. The lines are guides to the eye.

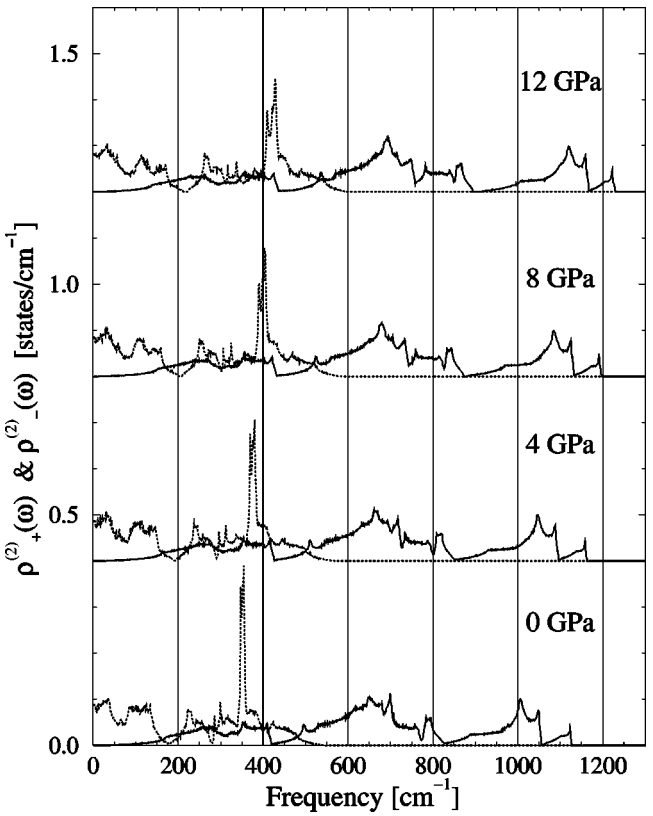


FIG. 4. Like Fig. 2 but for the zinc-blende structure.

should belong to the Γ-L-H region. The calculated frequency for the difference mode is 290 cm$^{-1}$ for natural isotopic abundances and its pressure coefficient 3 cm$^{-1}$/GPa, which agrees reasonably well with the measured pressure coefficient, also 3 cm$^{-1}$/GPa. The calculated frequencies for natural ZnO must be converted to those which would correspond to $^{64}Zn^{18}O$ for comparison with measurements of the isotopically pure crystal. This conversion reduces the LO$-B_1$ frequency to 280 cm$^{-1}$, considerably lower than the experimental value of 302 cm$^{-1}$. The discrepancy can be eliminated by correcting for the 25 cm$^{-1}$ difference between the calculated and experimental values of the LO Raman frequencies. Similar two peaks, related to difference modes, have also been found in Raman spectra of wurtzite-GaN.[72]

In order to obtain additional support for the assignment above, we discuss the differences in the frequencies we measured for $^{64}Zn^{18}O$ and $^{64}Zn^{16}O$. We find for the $E_2^{\mathrm{high}}-E_2^{\mathrm{low}}$ difference a blue shift of $+21(1)$ cm$^{-1}$ and for the weaker LO$-B_1$ a shift of $+23(3)$ cm$^{-1}$. These shifts agree satisfactorily with the calculated values, 22 and 25 cm$^{-1}$, respectively.

#### *2. Zinc blende*

The $\rho_+^{(2)}(\omega)$ and $\rho_-^{(2)}(\omega)$ calculated for the zinc-blende phase of ZnO at several pressures for a total $\mathbf{q}=0$ are shown in Fig. 4. As expected, they are rather similar to those displayed for the wurtzite structure in Fig. 2. This also applies to the pressure dependence of both DOS. The only striking difference is the fact that for wurtzite the DOS have many more critical points than for the zinc-blende structure (see, e.g., the band centered at 400 cm$^{-1}$ in Figs. 2 and 3). This results from the fact that wurtzite has twice as many bands as zinc blende in the first BZ and, correspondingly, a larger number of critical points. Moreover, the lower symmetry of wurtzite produces splitting of all doubly degenerate modes of zinc blende except those along the $c$ axis. $\rho_-^{(2)}(\omega)$ also shows a dominant peak at 350 cm$^{-1}$ at zero pressure which corresponds to TO$-$TA differences and is very similar to the TO$-E_2^{\mathrm{low}}$ peak of wurtzite.

#### *3. Rocksalt*

The sum and difference two-phonon DOS of ZnO are displayed in Fig. 5 for several pressures. All structures shift up in frequency with increasing pressure, thus reflecting the positive pressure derivatives of the frequencies given in Table VIII. This is also supported by the blue shift of the phonon-dispersion relations with pressure displayed in Fig. 1(c). The first-order spectra of the rocksalt structure are not Raman allowed. Therefore it may be possible to see clearly the second-order Raman spectra without contamination of strong first-order peaks, which could be investigated separately using infrared absorption. The DOS shown in Fig. 5 should help future investigations of second-order Raman spectra of ZnO above the phase transition. It is interesting to

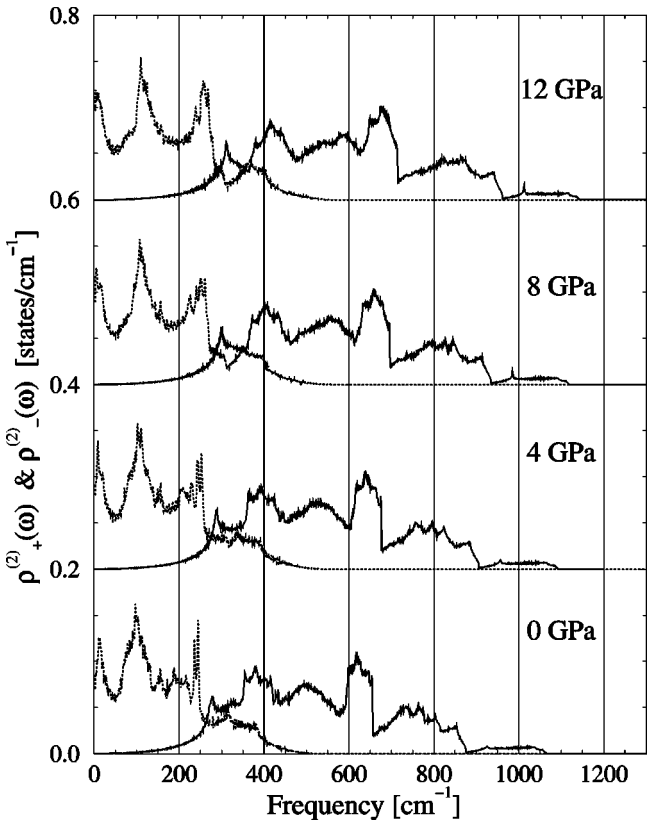


FIG. 5. Like Fig. 2 but for the rocksalt structure.

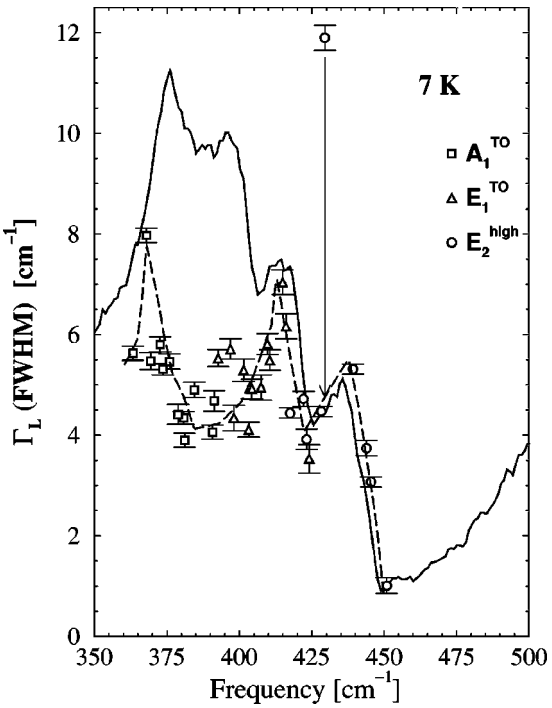


FIG. 6. Phonon linewidth (FHWM) of $A_1^{\mathrm{TO}}$, $E_1^{\mathrm{TO}}$, and $E_2^{\mathrm{high}}$ vs Raman shift. Data extracted from measurements at 7 K on samples with several isotopic compositions (Refs. 32 and 86). The point separated by an arrow corresponds to the $E_2^{\mathrm{high}}$ mode for $^{\mathrm{nat}}\mathrm{Zn}^{16}\mathrm{O}^{18}_{0.5}\mathrm{O}_{0.5}$, the arrow length indicating the additional broadening due to isotopic-mass disorder [see Eq. (4)]. The solid curve is the calculated two-phonon (sum) DOS, shifted by $+10$ cm$^{-1}$ and multiplied by an anharmonic coupling constant of 57 cm$^{-2}$, as explained in the text and in Ref. 32. The dashed curve has been plotted through the measured points as a guide to the eye.

note that the TO modes of this structure nearly overlap with a strong peak in $\rho^{(2)}_-(\omega)$ in Fig. 5. Therefore it is expected that decay of the ir-active TO mode into the corresponding difference mode should yield a significant contribution to the linewidth of the former at finite temperatures. At low temperature, this contribution should vanish on account of the Bose-Einstein statistical factors, as discussed next.

### C. Anharmonic phonon linewidths: dependence on pressure and isotopic mass

Besides the isotopic disorder induced linewidths of the $\Gamma$ phonons, discussed in Sec. IV A 2, one must consider the effects of anharmonic decay. The FWHM is directly related to the two-phonon DOS

$$\Gamma_+(\omega)=|V_3^+|^2\,\rho_+^{(2)}(\omega)[1+n_{\mathrm{BE}}(\omega_1)+n_{\mathrm{BE}}(\omega_2)], \quad (5a)$$

$$\Gamma_-(\omega)=|V_3^-|^2\,\rho_-^{(2)}(\omega)[n_{\mathrm{BE}}(\omega_1)-n_{\mathrm{BE}}(\omega_2)], \quad (5b)$$

where $V_3^+$ and $V_3^-$ are third-order anharmonic coupling constants, expected to depend only weakly on frequency, and $n_{\mathrm{BE}}(\omega)$ are the Bose-Einstein factors. In Eq. (5b) we have assumed that $\omega_1<\omega_2$. Strong dependence of the FWHM on frequency, and its pressure dependence, usually results from the critical-point structure in the pressure dependent two-phonon DOS, shown in Fig. 2.

Of particular interest is the behavior of the widths of the $E_2^{\mathrm{high}}$ phonon, whose frequency falls on the ridge of $\rho_+^{(2)}(\omega)$, which can be seen in Fig. 2 below the near gap at 440 cm$^{-1}$. This, and the dependence of the FWHM on isotopic mass, has been discussed in detail in Ref. 32. We reproduce in Fig. 6 some of the data of that reference for the $E_2^{\mathrm{high}}$ modes, together with our new data for the $A_1^{\mathrm{TO}}$ and $E_1^{\mathrm{TO}}$ modes. The representation of this figure has been conceived in the manner described in Ref. 32 so as to refer all experimental points to a single $\rho_+^{(2)}(\omega)$, which corresponds to ambient pressure and a fixed isotopic composition. The FWHM of the $E_2^{\mathrm{high}}$ mode shown in Fig. 6 follows very well the prediction of Eq. (5a) with $|V_3^+|^2=57$ cm$^{-2}$ whereas the widths of the $A_1^{\mathrm{TO}}$ and $E_1^{\mathrm{TO}}$ modes deviate somewhat from it, even if one readjusts the value of $|V_3^+|^2$. An average value of $|V_3^+|^2=50$ cm$^{-2}$ gives the best overall agreement in the $A_1^{\mathrm{TO}}$-$E_1^{\mathrm{TO}}$ region. The most conspicuous discrepancy between the theoretical and experimental frequency dependence is the lack of a peak at 395 cm$^{-1}$ in the latter. The reason may be inaccuracies in the calculated dispersion relations for the corresponding TA and/or LA modes. It is conceivable that, if this inaccuracy is corrected, the 395 cm$^{-1}$ peak may be brought very close to the one at 415 cm$^{-1}$, thus enhancing the height of the latter and reproducing the experimental results rather well. The point representing a width of 12 cm$^{-1}$ in Fig. 6 corresponds to a $^{\mathrm{nat}}\mathrm{Zn}^{16}\mathrm{O}^{18}_{0.5}\mathrm{O}_{0.5}$ crystal.[32] The effect

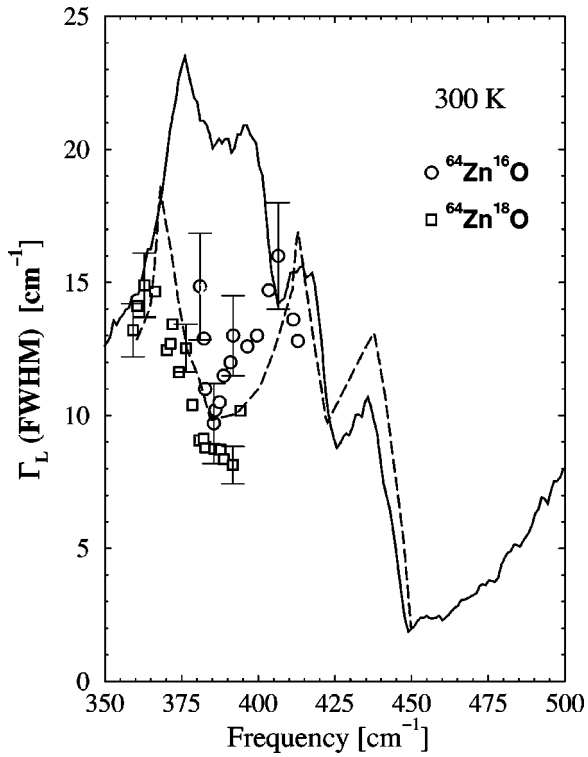


FIG. 7. Representation of the change of FWHM of the $A_1^{TO}$ modes vs frequency extracted from room-temperature Raman measurements under pressure on samples of $^{64}Zn^{16}O$ (solid circles) and $^{64}Zn^{18}O$ (solid squares), in a similar way as in Ref. 32. The solid curve represents the anharmonic FWHM obtained from Eq. (5a) using $|V_3^+|^2=50$ cm$^{-2}$ and the appropriate Bose-Einstein factors (see text). The dashed curve is the guide to the eye of Fig. 6, multiplied by the Bose-Einstein factors described in the text (a factor of 2.4).

of isotopic disorder on the FWHM, equal to 7 cm$^{-1}$ according to this figure, has been discussed in Sec. IV A 2 where a calculated value of 5 cm$^{-1}$ was reported. We note that this sample shows negligible isotopic broadening for the $A_1^{TO}$ and $E_1^{TO}$ modes. The reason is to be found in the one-phonon DOS of Fig. 1(a): The frequencies of these modes fall at the top of the acoustic-optic gap, in a region where there are basically no states available for elastic scattering.

The analysis given above for the $A_1^{TO}$ and $E_1^{TO}$ widths is supported by our Raman measurements under pressure on two isotopically pure samples: $^{64}Zn^{18}O$ and $^{64}Zn^{16}O$ (for details on the experimental method see Ref. 32). With the representation used in Fig. 6 we obtain, at room temperature, the results displayed in Fig. 7. According to Eq. (5a), $\rho_+^{(2)}(\omega)$ has been multiplied by the Bose-Einstein factors which correspond to the average TA and LA decay frequencies of 150 and 250 cm$^{-1}$. The best-fit results in an average $|V_3^+|^2=50$ cm$^{-2}$. Comparison in Fig. 2 of $\rho_+^{(2)}(\omega)$ and $\rho_-^{(2)}(\omega)$ at the frequency of the $E_2^{low}$ mode (100 cm$^{-1}$) suggests that the only significant anharmonic broadening mechanism corresponds to difference modes, which have a strong peak at that frequency. According to Eq. (5b), this mechanism should vanish at low temperatures, at which the FWHM should be due to isotopic disorder, as discussed in Sec. IV A 2. For an isotopically natural sample this FWHM was calculated to be 0.06 cm$^{-1}$, as compared to measurements indicating that this FWHM is smaller than 0.1 cm$^{-1}$.[63]

## V. CONCLUSIONS

Pseudopotential LDA electronic structures have been used to calculate structural parameters, bulk moduli, and transition pressures of ZnO in three modifications: the conventional wurtzite, the nearly isoenergetic zinc blende, and the first high-pressure phase (rocksalt). The pressure for the wurtzite-to-rocksalt transition has been evaluated. The structural parameters and bulk moduli have been compared with experimental data, whereby emphasis has been placed in removing from the latter the anharmonic effects, in particular, the zero-point renormalizations which account for part of the discrepancies between theory and experiments.

The LDA electronic structures have also been used to calculate the phonon-dispersion relations of the three modifications, including phonon eigenvectors, their pressure dependence, and a few additional response properties such as $\epsilon_\infty$ and the effective charges and their dependence on pressure. The one- and two-phonon densities of states have been also calculated and used for analysis of the isotopic disorder induced and anharmonic contributions to the linewidth of the Raman phonons. By comparison with experimental data, especially those obtained by applying a hydrostatic pressure and/or varying the isotopic masses, very detailed information on the mechanisms contributing to the linewidths has been obtained. The two-phonon DOS have been used to interpret extant second-order Raman spectra.

It is hoped that this work will encourage additional experiments on phonon linewidths and second-order Raman measurements, especially for the rocksalt modification of ZnO, as well as detailed measurements for the phonon-dispersion relations of the wurtzite modification, which could be performed using INS or inelastic x-ray scattering. The latter has been recently employed to obtain the dispersion relations of wurtzite-type GaN.[81]

## ACKNOWLEDGMENTS

Thanks are due to K. Syassen for allowing us to use his high-pressure and spectrometer system and also for many stimulating discussions. J.S. acknowledges partial support from DIPC. A.H.R. acknowledges support from Millennium Conacyt, Initiative Mexico under Grant No. W-8001. F.J.M. acknowledges financial support from the ''Programa Incentivo a la Investigacion de la UPV,'' the MCYT Grant No. MAT2002-04539-C02-02, and the Generalitat Valenciana OCYT Grant No. GV01-211. A.R. was partially supported by DGES, University of the Basque Country (Grant No. 9/UPV 00206.215-13639/2001) and EC-RTN programs Nanophase (Grant No. HPRN-CT-2000-00167) and Comelcan (HPRN-CT-2000-00128), and by the Spanish MCyT (Grant No. MAT2001-0946). Computer time has been granted by the Center de Computació i Comunicacions de Catalunya ($C^4$).

*Corresponding author. Email address: m.cardona@fkf.mpg.de

[1] D.R. Clarke, J. Am. Ceram. Soc. **82**, 485 (1999).
[2] H. E. Brown, *Zinc oxide: Properties and Applications* (Pergamon Press, New York, 1976).
[3] It seems to stimulate feed intake and weight increase of weanling pigs. For more information see http://hoginfo.com/pubs/Topics/Nursery_Management/Feed_aditives
[4] G.M. Hill, G.L. Cromwell, T.D. Crenshaw, C.R. Dove, R.C. Ewan, D.A. Knabe, A.J. Lewis, G.W. Libal, D.C. Mahan, G.C. Shurson, L.L. Southern, and T.L. Veum, J. Anim. Sci. (Savoy, Ill.) **78**, 1010 (2000).
[5] F. Hamdani, A. Botchkarev, W. Kim, H. Morkoc, M. Yeadow, J.M. Gibson, S.C.Y. Tsen, D.J. Smith, K. Evans, C.W. Litton, W.C. Michel, and P. Hemenger, Appl. Phys. Lett. **70**, 467 (1997).
[6] A. Ohtomo, M. Kawasaki, I. Ohkubo, H. Koinuma, T. Yasuda, and Y. Segawa, Appl. Phys. Lett. **75**, 980 (1999).
[7] Y.-N. Xu and W.Y. Ching, Phys. Rev. B **48**, 4335 (1993).
[8] P. Schröer, P. Krüger, and J. Pollmann, Phys. Rev. B **47**, 6971 (1993).
[9] J.E. Jaffe, J.A. Snyder, Z. Lin, and A.C. Hess, Phys. Rev. B **62**, 1660 (2000).
[10] M. Oshikiri and F. Aryasetiawan, Phys. Rev. B **60**, 10754 (1999).
[11] M. Oshikiri and F. Aryasetiawan, J. Phys. Soc. Jpn. **69**, 2113 (2000).
[12] R. Helbig, J. Cryst. Growth **15**, 25 (1972).
[13] A.W. Hewat, Solid State Commun. **8**, 187 (1970).
[14] W. Wegener and S. Hautecler, Phys. Lett. **31A**, 2 (1970).
[15] K. Thoma, B. Dorner, G. Duesing, and W. Wegener, Solid State Commun. **15**, 1111 (1974).
[16] T.C. Damen, S.P.S. Porto, and B. Tell, Phys. Rev. **142**, 570 (1966).
[17] S.P.S. Porto, B. Tell, and T.C. Damen, Phys. Rev. Lett. **16**, 450 (1966).
[18] J.M. Calleja and M. Cardona, Phys. Rev. B **16**, 3753 (1977).
[19] B.H. Bairamov, A. Heinrich, G. Irmer, V.V. Toporov, and E. Ziegler, Phys. Status Solidi B **119**, 227 (1983).
[20] D.G. Mead and G.R. Wilkinson, J. Raman Spectrosc. **6**, 123 (1977).
[21] F. Decremps, J. Pellicer-Porres, A.M. Saitta, J.-C. Chervin, and A. Polian, Phys. Rev. B **65**, 092101 (2002).
[22] F.J. Manjón, K. Syassen, and R. Lauck, High Press. Res. **22**, 299 (2002).
[23] J.W. Orton and C.T. Foxon, Rep. Prog. Phys. **61**, 1 (1998), and references therein.
[24] H. Karzel, W. Potzel, M. Köfferlein, W. Schiessl, M. Steiner, U. Hiller, G.M. Kalvius, D.W. Mitchell, T.P. Das, P. Blaha, K. Schwarz, and M.P. Pasternak, Phys. Rev. B **53**, 11425 (1996).
[25] S. Desgreniers, Phys. Rev. B **58**, 14102 (1998).
[26] A. Mujica, A. Rubio, A. Muñoz, and R.J. Needs, Rev. Mod. Phys. **75**, 863 (2003).
[27] A.B.M.A. Ashrafi, A. Ueta, A. Avramescu, H. Kumano, I. Suemune, Y.W. Ok, and T.Y. Seong, Appl. Phys. Lett. **76**, 550 (2000).
[28] W.H. Bragg and J.A. Darbyshire, Trans. Faraday Soc. **28**, 252 (1932).
[29] F. Decremps, J. Pellicer-Porres, F. Datchi, J.P. Itié, A. Polian, F. Baudelet, and J.Z. Jiang, Appl. Phys. Lett. **81**, 4820 (2002).
[30] X. Gonze, Phys. Rev. B **55**, 10 337 (1997).
[31] S. Baroni, S. de Gironcoli, A. DalCorso, and P. Giannozzi, Rev. Mod. Phys. **73**, 515 (2001).
[32] J. Serrano, F.J. Manjón, A.H. Romero, F. Widulle, R. Lauck, and M. Cardona, Phys. Rev. Lett. **90**, 055510 (2003).
[33] X. Gonze, J.-M. Beuken, R. Caracas, F. Detraux, M. Fuchs, G.-M. Rignanese, L. Sindic, M. Verstraete, G. Zerah, F. Jollet, M. Torrent, A. Roy, M. Mikami, Ph. Ghosez, J.Y. Raty, and D.C. Allan, Comput. Mater. Sci. **25**, 478 (2002).
[34] The ABINIT code is a common project of the Université Catholique de Louvain, Corning Incorporated, and other contributors, URL http://www.abinit.org
[35] W.E. Pickett, Comput. Phys. Rep. **9**, 115 (1989).
[36] N. Troullier and J.L. Martins, Phys. Rev. B **43**, 1993 (1991).
[37] D.M. Ceperley and B.J. Alder, Phys. Rev. Lett. **45**, 566 (1980).
[38] J.P. Perdew and A. Zunger, Phys. Rev. B **23**, 5048 (1981).
[39] L. Hedin, Phys. Rev. **139**, A796 (1965).
[40] F. Aryasetiawan and O. Gunnarsson, Rep. Prog. Phys. **61**, 237 (1998).
[41] G. Onida, L. Reining, and A. Rubio, Rev. Mod. Phys. **74**, 601 (2002).
[42] A. Mang, K. Reimann, and S. Rubenacke, Solid State Commun. **94**, 251 (1995).
[43] H.J. Monkhorst and J.D. Pack, Phys. Rev. B **8**, 5747 (1973).
[44] X. Gonze and C. Lee, Phys. Rev. B **55**, 10355 (1997).
[45] G.D. Archard, Acta Crystallogr. **6**, 657 (1953).
[46] T. Lei, M. Fanciulli, R.J. Molnar, and T.D. Moustakas, Appl. Phys. Lett. **59**, 944 (1991).
[47] J.H. Edgar, J. Mater. Res. **7**, 235 (1992).
[48] J.E. Jaffe and A.C. Hess, Phys. Rev. B **48**, 7903 (1993).
[49] J. Albertsson, S.C. Abrahams, and A. Kvick, Acta Crystallogr., Sect. B: Struct. Sci. **B45**, 34 (1989).
[50] M. Cardona, in *Electrons and Photons in Solids, A Volume in Honour of Franco Bassani* (Scuola Normale, Pisa, 2001), p. 25.
[51] Landolt-Börnstein, *Numerical Data and Functional Relationships in Science and Technology*, edited by O. Madelung, U. Rössler, and M. Schulz, New Series, Group III, Vols. 17b, 22a, and 41b, Pt. a (Springer, Berlin, 1999).
[52] H.M. O'Bryan, Jr., L.G.V. Uitert, E.D. Kolb, and G. Zydzik, J. Am. Ceram. Soc. **61**, 269 (1978).
[53] The phonon renormalization of the lattice constant at 0 K is defined as $\Delta a/a|_{\text{renorm}} = \Delta a/a|_{0\text{K}} - \Delta a/a|_{\text{bare}}$, where $\Delta a/a|_{\text{bare}}$ is obtained from the linear extrapolation to $T=0$ K of the temperature dependence of the lattice constant at high temperatures. The unrenormalized (bare) values are those which correspond to atoms in fixed positions, i.e., not subject to either thermal or zero-point vibrations.
[54] R.R. Reeber and K. Wang, J. Electron. Mater. **25**, 63 (1996).
[55] E. Sozontov, L.X. Cao, A. Kazimirov, V. Kohn, M. Konuma, M. Cardona, and J. Zegenhagen, Phys. Rev. Lett. **86**, 5329 (2001).
[56] J.B. Kobiakov, Solid State Commun. **35**, 305 (1980).
[57] W.H. Bragg and J.A. Darbyshire, J. Meteorol. **6**, 238 (1954).
[58] F. Decremps, J. Zhang, B. Li, and R.C. Liebermann, Phys. Rev. B **63**, 224105 (2001).
[59] A. Zaoui and W. Sekkal, Phys. Rev. B **66**, 174106 (2002).
[60] S. Limpijumnong and W.R.L. Lambrecht, Phys. Rev. Lett. **86**, 91 (2001).
[61] J.M. Recio, M.A. Blanco, V. Luaña, R. Pandey, L. Gerward, and J.S. Olsen, Phys. Rev. B **58**, 8949 (1998).

[62] K. Kusaba, Y. Syono, and T. Kikegawa, Proc. Jpn. Acad., Ser. B: Phys. Biol. Sci. **75**, 1 (1999).
[63] J. Serrano, F. Widulle, A.H. Romero, M. Cardona, R. Lauck, and A. Rubio, Phys. Status Solidi B **235**, 260 (2003).
[64] F. Widulle, T. Ruf, M. Konuma, I. Silier, M. Cardona, W. Kriegseis, and V.I. Ozhogin, Solid State Commun. **118**, 1 (2001).
[65] J. Serrano, A. Cantarero, M. Cardona, N. Garro, R. Lauck, R.E. Tallman, T.M. Ritter, and B.A. Weinstein, Phys. Rev. B **69**, 014301 (2004).
[66] E. Anastassakis and M. Cardona, in *High Pressure Semiconductor Physics II, Semiconductors and Semimetals*, edited by T. Suski and W. Paul (Academic Press, New York, 1998), Vol. 55, p. 117.
[67] B. A. Weinstein and R. Zallen, in *Light Scattering in Solids*, edited by M. Cardona and G. Güntherodt (Springer, Berlin, 1984), Vol. IV, pp. 463–527.
[68] T. H. K. Barron and M. L. Klein, in *Dynamical Properties of Solids*, edited by G. K. Horton and A. A. Maradudin (North-Holland, Amsterdam, 1974), Vol. 1, p. 418.
[69] D.P. Penn, Phys. Rev. **128**, 2093 (1962).
[70] O. Zakharov, A. Rubio, X. Blase, M.L. Cohen, and S.G. Louie, Phys. Rev. B **50**, 10780 (1994).
[71] K. Vedam and T.A. Davis, Phys. Rev. **181**, 1196 (1969).
[72] U. Haboeck, H. Siegle, A. Hoffmann, and C. Thomsen, Phys. Status Solidi C **0**, 1710 (2003).
[73] A. Debernardi and M. Cardona, Phys. Rev. B **54**, 11305 (1996).
[74] O. Blaschko, G. Ernst, G. Quittner, W. Kress, and R.E. Lechner, Phys. Rev. B **11**, 3960 (1975).
[75] G. Ernst, G. Krexner, G. Quittner, W. Kress, B. Buras, and B. Lebech, Phys. Rev. B **29**, 5805 (1984).
[76] S. Klotz (private communication).
[77] A. Zunger, K. Kim, and V. Ozolins, Phys. Status Solidi B **223**, 369 (2001).
[78] A. Segura, J.A. Sans, F.J. Manjón, A. Muñoz, and M.J. Herrera-Cabrera, Appl. Phys. Lett. **83**, 278 (2003).
[79] F. Widulle, J. Serrano, and M. Cardona, Phys. Rev. B **65**, 075206 (2002).
[80] O. Brafman and S. S. Mitra, in *Light Scattering in Solids*, edited by M. Balkanski (Flammarion, Paris, 1971), p. 284.
[81] T. Ruf, J. Serrano, M. Cardona, P. Pavone, M. Pabst, M. Krisch, M. D'Astuto, T. Suski, I. Grzegory, and M. Leszczynski, Phys. Rev. Lett. **86**, 906 (2001).
[82] G. Lucovsky, R.M. Martin, and E. Burstein, Phys. Rev. B **4**, 1367 (1971).
[83] The effective charge is calculated in Ref. 82 by taking $\overline{\omega_{LO}^2} = \frac{1}{3}[\omega_{LO}^2(A_1) + 2\omega_{LO}^2(E_1)]$, and similarly for the TO phonons.
[84] A. DalCorso, M. Posternak, R. Resta, and A. Baldereschi, Phys. Rev. B **50**, 10715 (1994).
[85] F. Bernardini, V. Fiorentini, and D. Vanderbilt, Phys. Rev. B **56**, R10024 (1997).
[86] J. Serrano, Ph.D. thesis, Universität Stuttgart, 2003 (unpublished).